BULETINUL INSTITUTULUI POLITEHNIC DIN IAŞI
Publicat de
Universitatea Tehnică „Gheorghe Asachi” din Iaşi
Volumul 69 (73), Numărul 3, 2023
Secţia
CONSTRUCŢII DE MAŞINI
DOI:10.2478/bipcm-2023-0025

IMPROVING INSTANTANEOUS ANGULAR SPEED MONITORING BY MEANS OF SINUSOIDAL EMF SIGNALS DELIVERED BY A TWO-PHASE *n* POLES AC GENERATOR USED AS A SENSOR

BY

MOHAMMED KHDAIR, CONSTANTIN-GHEORGHE MIHAI, NECULAI-EDUARD BUMBU, MIHĂIȚĂ HORODINCĂ*

“Gheorghe Asachi” Technical University of Iaşi,
Faculty of Machine Manufacturing and Industrial Management,
Digital Manufacturing Systems Department, Iași, Romania

Received: December 10, 2023
Accepted for publication: December 20, 2023

Abstract. This paper introduces a new approach in instantaneous angular speed monitoring using a two-phase *n* poles AC generator as sensor. A two-phase *n* poles (*n=50*) stepper motor plays the role of sensor. Its rotor is firmly connected to the rotary part whose instantaneous angular speed should be measured. The sensor produces two identical sinusoidal EMF (electromotive force) signals (theoretically shifted with *π/2* radians) with the same periods *T*. This paper proposes to use the mathematical product of the numerical descriptions of these EMF signals in order to define a new EMF signal with a period *T/2* whose analysis allows the determination *of 4·n=200* samples of instantaneous angular velocity on each full rotation. Each period of this new EMF signal (with an overlap of a semi period) is involved in the description of the instantaneous angular speed. In this way, the sensor is virtually converted in a single-phase *2·n* poles (*2·n=100*) AC generator. The experimental results confirm the validity of this approach.

*Corresponding author; *e-mail*: horodinca@tuiasi.ro.
© 2023 Mohammed Khdair et al.
This is an open access article licensed under the Creative Commons Attribution-NonCommercial-NoDerivatives 4.0 International License (CC BY-NC-ND 4.0).

Keywords: Instantaneous angular speed, measuring method, AC generator, sinusoidal EMF signal, signal processing.

1. Introduction

Instantaneous angular speed (IAS) monitoring is a useful issue in monitoring the condition of transient and stationary regimes on rotary machines.

This is due to a specific behaviour known to any type of electric drive motor used to actuate these machines: any normal or abnormal temporary increasing (decreasing) of mechanical loading (as torque or moment of force) produces the decreasing (increasing) of IAV according to the speed-torque characteristic of the motor.

Some different techniques of IAS monitoring was already developed before (Horodincă *et al.*, 2020; Ciurdea and Horodincă, 2017; Lei *et al*., 2014; Li *et al*., 2017) using different types of sensors, as rotary encoders (Bourdon *et al.*, 2014), rotary resolvers (Sarma *et al.*, 2008; Bourogaoui *et al.*, 2016), variable reluctance sensors (Kim *et al.*, 2007; Guo *et al.*, 2017), a quadrature sine and cosine signals generator (Zhao *et al.*, 2018) or a two-phases *n* poles AC generator (Horodincă *et al.*, 2020; Ciurdea and Horodincă, 2018). Generally these measurement techniques use the time elapsed method (Li *et al*., 2005): an angle divided by time interval defines an IAS sample. Except the achievements from (Horodincă *et al*., 2020; Zhao *et al*., 2018), the number of IAS samples per sensor rotation is relatively small.

This paper proposes an improvement of an approach already proposed in (Ciurdea and Horodincă, 2017). Here a two-phase $n=50$ poles stepper motor was used as AC generator (sensor). The time delay interval between each two successive zero-crossing moments of the sinusoidal EMF (electromotive force) signal generated by a single phase is used to calculate the signal semi-period and describe the IAS evolution. In this approach $2 \cdot n=100$ IAS samples per rotation are available (for $2 \cdot n$ EMF semi-periods per rotation). In a new approach, a mathematical product of the numerical descriptions of both sinusoidal EMF signals (having the periods T, with a phase shift of $\pi/2$) defines a single (theoretical) sinusoidal EMF signal (as NEFM, having the period $T/2$). Now the sensor is virtually converted in a single-phase $2 \cdot n$ poles AC generator. Each semi-period of the NEFM signal is involved now in IAS definition. There are $4 \cdot n=200$ semi-periods in NEFM signal so 200 IAS samples per sensor rotation are available. Because the NEMF signal is not strictly sinusoidal (it has a DC offset because the phase shift in between EMF signals is not exactly $\pi/2$) it was found that in the IAS description it is more appropriate to use NEMF periods but with a semi-period overlap between each two successive periods.

The next sections of this paper are organized as follows: Section 2 presents a theoretical approach, Section 3 briefly presents the experimental setup,

Section 4 presents the experimental results and discussion and Section 5 presents the conclusion and the future work.

2. A Theoretical Approach

Suppose that the two sinusoidal EMF signals e_1, e_2 delivered by the sensor phases have (ideally, as desired) strictly the same amplitude (a) and $\pi/2$ phase shift between them and the sensor rotor rotates with a constant IAS ω. The EMF signals can be described as:

$$e_1 = a\sin(n\omega t) \qquad e_2 = a\cos(n\omega t) \tag{1}$$

Their mathematical product (e_1e_2) describes the sinusoidal NEMF signal written as:

$$e_1e_2 = a^2\sin(n\omega t)\cos(n\omega t) \tag{2}$$

A trigonometric formula ($\sin(\alpha+\beta) = \sin(\alpha)\cos(\beta)+\sin(\beta)\cos(\alpha)$ rewritten as $\sin(2\alpha)=\sin(\alpha)\cos(\alpha)+\sin(\alpha)\cos(\alpha)=2\sin(\alpha)\cos(\alpha)$) allows (if we consider that $\alpha= n\omega t$) to rewrite the description of NEMF signal from Eq. (2) as:

$$e_1e_2 = a^2\sin(n\omega t)\cos(n\omega t) = \frac{a^2}{2}\sin(2n\omega t) \tag{3}$$

It is obviously here that the EMF signal has an $n\omega$ angular frequency (hence the period $T_{EMF}=2\pi/n\omega$) while the NEMF has a $2n\omega$ angular frequency (hence the period $T_{NEMF}=2\pi/2n\omega$), with $T_{NEMF}=T_{EMF}/2$. For each period of an EMF signal (or n periods T_{EMF} per sensor rotor revolution as well) there are two periods of NEMF (or $2n$ periods T_{NEMF} per sensor rotor revolution as well). The NEMF frequency is two times greater than EMF frequency. This is proved in the graphical simulation (in Matlab) from Fig. 1 (for $a=b=2V$, $\omega=2\pi$ rad/s, so $T_{EMF}=1s$) with $t=0 \div T_{EMF}$. The evolutions of e_1, e_2 (EMF signals, from Eq. (1)) and their mathematical product e_1e_2 (as NEMF signal) are illustrated. At each time t a sample of NEMF is defined as the mathematical product of an e_1 sample with an e_2 sample.

It is obvious that Eq. (3) and the relationship $T_{NEMF}=T_{EMF}/2$ are fully confirmed. Each period T_{EMF} have two semi-periods. There are $n=50$ periods T_{EMF} and $2n=100$ semi-periods for each full rotation, so 100 IAS samples can be defined using an EMF signal (as IAS_1 method). However, if both EMF signals are used (as IAS_{1a} method), then 200 IAS_{1a} samples can be defined: a sample is defined using a semi-period of an EMF signal, next sample is defined with next semi-period on the other EMF signal (with $T_{EMF}/4$ overlap).

For the same duration T_{EMF} there are four semi-periods T_{sNEMF} on NEMF signal and $2n=200$ semi-periods for each full sensor rotation, so 200 IAS samples can be defined this time (as IAS_2 method).

In order to detect the IAS_2 samples from NEMF signal, it is necessary to accurately detect its zero-crossing moments, an issue described in (Horodincă *et. al.* 2020). The time between two successive zero crossing moments of NEMF depicts a semi-period T_{sNEMF} which is involved in the description of a sample of IAS_2 as $\omega=2\pi/4nT_{sNEMF}$.

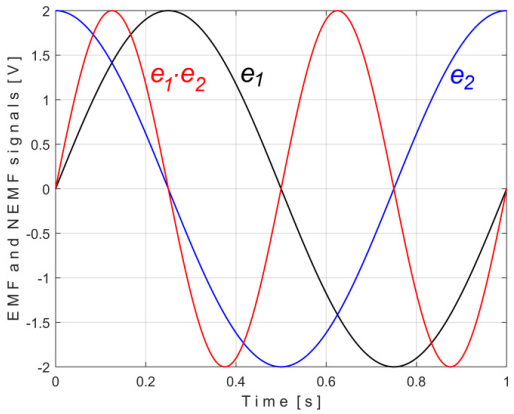


Fig. 1 – Simulation of the evolution of EMF and NEMF signals.

The availability of the signal NEMF is the same even if the amplitude of the EMF signals e_1 and e_2 are different and IAS is variable (as will be shown later).

The main idea of this improvement came from an earlier study (Bumbu and Horodincă, 2022) related by the properties of the instantaneous power absorbed in an AC system: this instantaneous power is defined as the mathematical product of two phase shifted sinusoidal signals (instantaneous current and voltage) having the same frequency (period). The instantaneous power frequency is two times greater than the voltage frequency.

3. The Experimental Setup

In order to prove the availability of this new approach in IAS monitoring, a simple experimental setup was developed, briefly described in Fig. 2.

The stepper motor 1, which plays the role of the sensor, is firmly placed in the chuck of an electric hand drill 2 which plays the role of a rotary machine. During rotary motion, the first phase of sensor generates on the output wires w1, w2 the first EMF signal (e_1) which is delivered (through a first oscilloscope probe) to the input channel A of the numerical oscilloscope 3 (PicoScope 4000

series from Pico Technology UK, 8 channels, 80 MS/s A/D conversion speed, 12 bits resolution, 256 MS buffer). Similarly, the second phase of sensor generates on the output wires w3, w4 the second EMF signal (e_2) which is delivered (through a second oscilloscope probe) to the input channel B of the numerical oscilloscope 3. The numerical description of EMF signals is delivered to a computer for data processing (NEMF synthesis, zero-crossing detection, semi-period time calculation, IAS samples calculus, etc.). In order to obtain high accuracy zero-crossing detection at high IAS, the sampling rate (sampling frequency) in numerical conversion of EMF (inside the oscilloscope) should be high enough in such a way to have a high number of samples on each EMF period (and NEMF period as well).

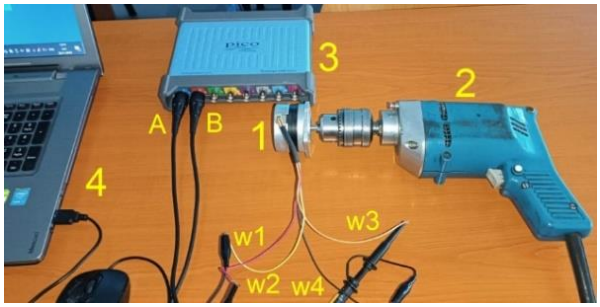


Fig. 2 – A view on the experimental setup. 1 – sensor; 2 – electric hand drill as rotary machine; 3 – numerical oscilloscope; 4 – computer; w1, w2 – wires for first EMF signal (e_1); w3, w4 – wires for second EMF signal (e_2); A, B – input channels in oscilloscope.

In our experiments, this sampling rate was 100,000 s^{-1}. For an average chuck frequency rotation of 52.5 Hz, there are 50·52.5=2,625 EMF periods and 2·50·52.5=5,250 NEMF periods per second (for 50 EMF periods and 100 NEMF periods on each rotation). This means that there are 100,000/2,625=38.09 samples per period on EMF and 100,000/5,250=19.045 samples per period on NEMF.

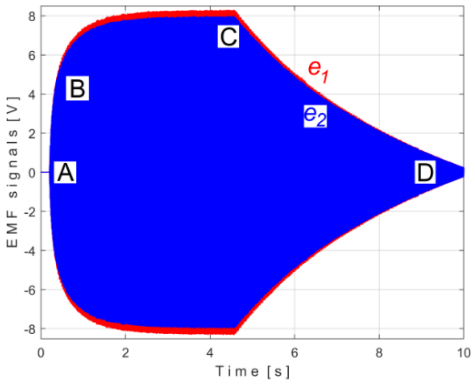


Fig. 3 – Description of the EMF signals delivered by the sensor during a transient regime of rotary motion.

It should be noted that the decrease in the number of samples per period (on NEMF compared to EMF) is an obvious disadvantage.

4. Experimental Results and Discussion

Figure 3 presents the evolutions of the EMF signals delivered by the sensor during an experiment made to describe the evolution of IAS in a transient-stationary regime. In A, the electric hand drill starts to rotate. A transient regime occurs in B with increasing of the rotation speed until C. In C the motor of electric hand drill is switched-off, the rotation speed slowly decreases until D, when the experiment ceases.

As it is clearly indicated, the amplitudes of EMF signals are not strictly the same (as a first fault of sensor, no effect on NEMF signal frequency). It is also obvious that the amplitude evolution of EMF signals is strictly related by IAS evolution, a topic already addressed before in (Ciurdea and Horodincă, 2018).

Figure 4 presents a zoom-in detail in the area A of Fig. 3 and some considerations related to IAS_1 method: the semi-periods of EMF signal e_1 (t_{11}, t_{12}, t_{13}, t_{14}...) are used successively in IAS_1 sample definition (as $\omega_{1i}=2\pi/2nt_{1i}$, with 100 samples per revolution).

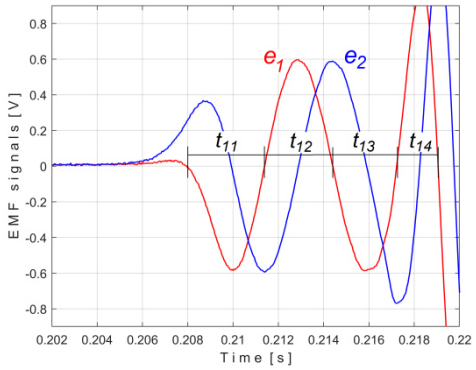


Fig. 4 – A highlighting of the semi-period involved in IAS_1 samples definition.

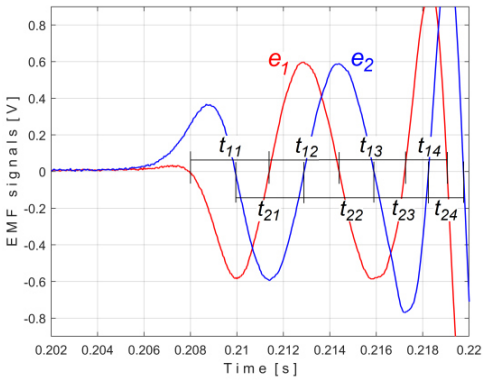


Fig. 5 – A highlighting of the semi-period involved in IAS_{1a} samples definition.

Figure 5 presents the same zoom-in detail and some considerations related to IAS_{1a} method: the semi-periods of EMF signals e_1 and e_2 are used in the succession t_{11}, t_{21}, t_{12}, t_{22}, t_{13}, t_{23} t_{14}, t_{24}... in IAS_{1a} sample definition (as $\omega_{1ai}=2\pi/4nt_{1i}$ if i is odd or as $\omega_{1ai}=2\pi/4nt_{2i}$ if i is even, with 200 samples per revolution).

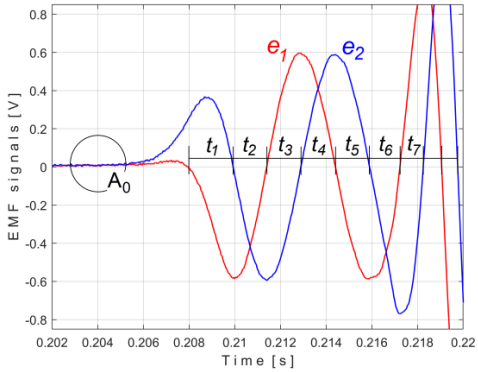


Fig. 6 – A highlighting of the time intervals involved in IAS_{1b} samples definition.

An alternative option for IAS_{1a} is presented in Fig. 6 as IAS_{1b}. It uses the successive time intervals (t_1, t_2, t_3, t_4……) between zero-crossing moments of EMF signals. A sample of IAS_{1b} is defined as $\omega_{1bi}=2\pi/4nt_i$ also with 200 samples per revolution.

Figure 7 presents a zoom-in detail in the same area A of Fig. 3 and some considerations related to IAS_2 method: the semi-periods (t_1, t_2, t_3, t_4...) of NEMF signal (represented in purple) are used successively in IAS_2 samples definition (as $\omega_{2i}=2\pi/4nt_i$, with 200 samples per revolution).

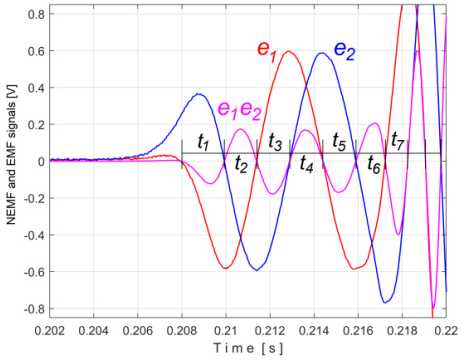


Fig. 7 – A highlighting of semi-periods involved in IAS_2 samples definition (zoom-in on area A from Fig. 3).

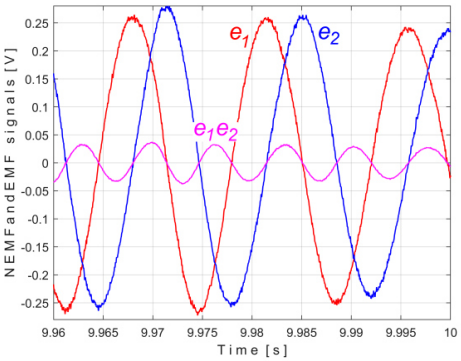


Fig.8 – A highlighting of semi-periods involved in IAS_2 samples definition (zoom-in on area D from Fig. 3).

Figure 8 presents the NEMF and EMF signals evolutions in the area D of Fig. 3. As expected NEMF signal keeps the same properties revealed before.

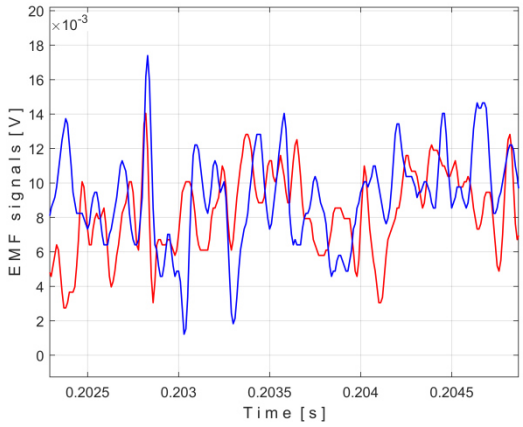


Fig. 9 – A zoom-in of area A_0 from Fig. 6.

In order to detect the zero-crossing moments of an EMF signal (to apply the IAS_1 method) or for the NEMF signal (to apply the IAS_2 method) a mandatory condition should be accomplished: the sensor rotor must be in rotational motion (in figure 7 after the first zero-crossing involved in t_1 definition). The DC offset on numerical description of the EMF signal (eventually generated by oscilloscope) should be removed. In order to avoid the appearance of false zero-crossing moments (because of electrical noise) both EMF signals should be slightly filtered (e. g. with a numerical low pass filter). Figure 9 present a zoom-in detail of area A_0 from Fig. 6. Here the DC offset (approx. 8 mV) and the electrical noise is revealed.

The EMF signal e_1 processing according to IAS_1 method for the evolution given in Fig. 3 is described in Fig. 10. It is obvious that the EMF (e_2) signal e_2 processing with the same method produces a very similar result (here superimposed over Fig. 10).

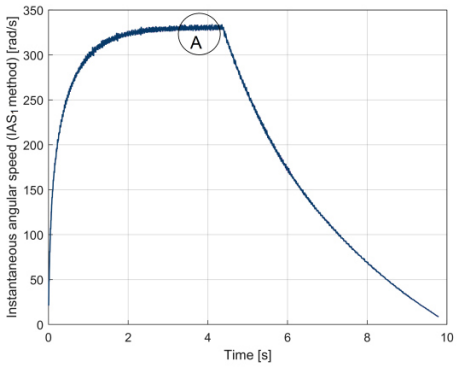


Fig. 10 – The IAS_1 evolution deduced from e_1 and e_2 EMF signals.

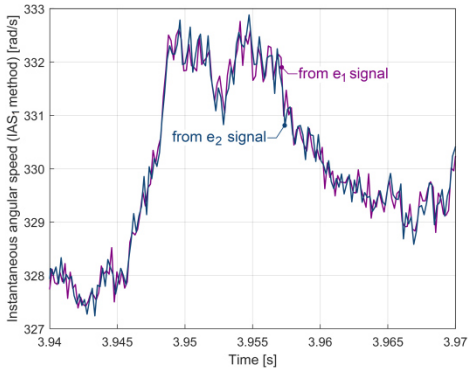


Fig. 11 – A zoom-in detail of 30 ms in area A from Fig. 10.

A zoom-in detail in area A from Fig. 10 is depicted in Fig. 11. As expected, both evolutions of IAS_1 are almost identical; with some (normal) minor differences (the EMF signals are not strictly identical, the time of samples is slightly different). This relatively strong variation of IAS_1 is related mainly by the behaviour of the rotary machine (useful in condition monitoring). We should

mention that the IAS_1 evolution is described by points (a point for each sample) and line segments between any successive two points.

The NEMF signal (e_1e_2) processing according with IAS_2 method is described in Fig. 12. This NEMF signal is generated by the mathematical product e_1e_2 of EMF signals already depicted in Fig. 3.

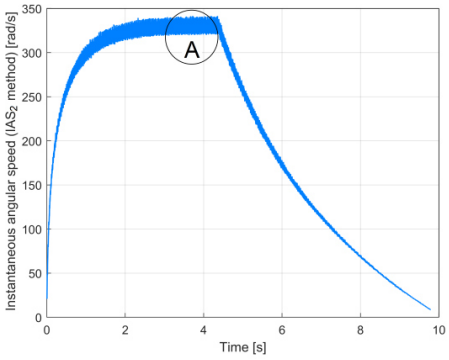


Fig. 12 – The IAS_2 evolution deduced from NEMF signal.

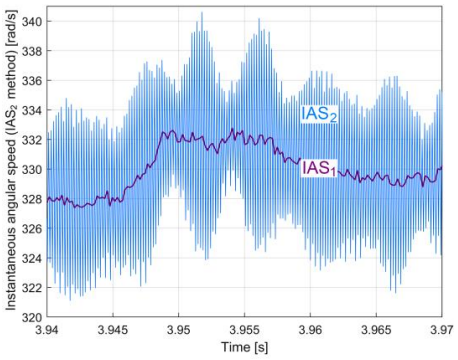


Fig. 13 – A zoom-in detail of 30 ms in area A from Fig. 12.

Figure 13 presents a zoom-in detail in area A from Fig. 12, with IAS_1 and IAS_2. It is obvious that IAS_2 contains a high amplitude variable component.

It is evident that this is a weakness in the application of this IAS_2 method. In order to find-out an explanation for this flaw, many hypotheses were tested. Finally, the exact reason was discovered: the EMF signals generated by the sensor e_1 and e_2 are not rigorously shifted with a phase shift of $\pi/2$. That is why a DC offset component occurs in NEMF definition. This is proved by simulation (Fig. 14), with a theoretical definition for e_1 and e_2 as:

$$e_1 = a\sin(n\omega t) \qquad e_2 = a\cos(n\omega t + \varphi) \tag{4}$$

In this new simulation the same values e_1, e_2, n and ω were used (as those already used in the simulation from Fig. 1), and $\varphi=-\pi/10$.

It is evident that a positive DC offset occurs, even if the IAS is constant, so a bad description of IAS it happens. As consequence, the positive semi-periods in NEFM increase and the negative ones decrease while their sum remains constant. This allows a new approach in IAS_2 definition (as IAS_{2a} method) which eliminates the inconvenient reported earlier in Fig.13: in the description of IAS_{2a}, the semi-periods are replaced by overlapped periods T_{NEMF1}, T_{NEMF2}, T_{NEMF3},...with IAS_{2a} samples defined as $\omega_i=2\pi/2nT_{NEMFi}$ (also with 200 samples per sensor rotor revolution).

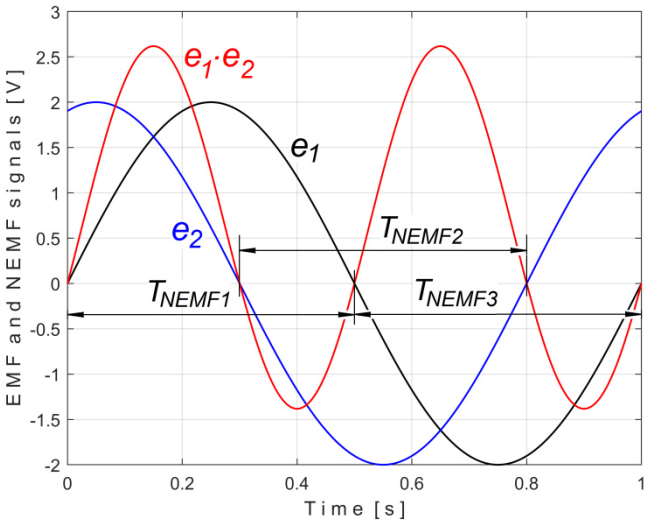


Fig. 14 –The occurrence of a DC offset component on the NEMF signal if the EMF signals are not rigorously shifted with $\pi/2$ (simulation).

The fact that e_1 and e_2 EMF signals are not rigorously shifted with a phase shift of $\pi/2$ is experimentally proved as it follows. A short sequence with these signals from Fig. 3 at $t \approx 4s$ is described in Fig. 15. Using *Curve fitter* application from Matlab, the best theoretical descriptions e_{1t} and e_{2t} of EMF signals were determined, as Eq. (5) and (6) describes.

$$e_{1t} = 7.948 \sin(16660 \cdot t - 0.08078) \tag{5}$$

$$e_{2t} = 8.237 \cos(16660 \cdot t + 1.494) \tag{6}$$

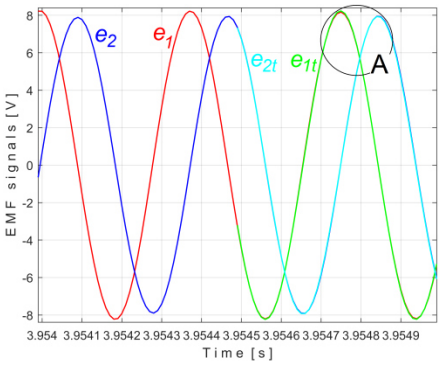


Fig. 15 – A sequence with experimental signals (e_1, e_2) and the best theoretical evolution (e_{1t}, e_{2t}) for EMF signals.

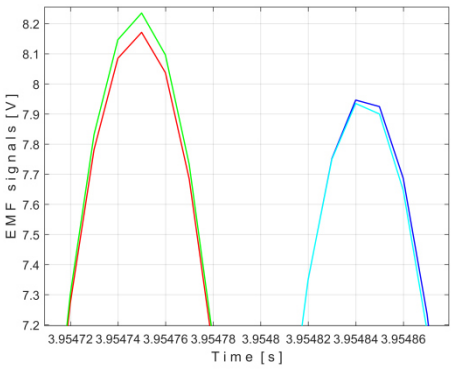


Fig. 16 – A zoom-in detail in area A from Fig. 15.

On the second half of Fig. 15, the e_{1t} and e_{2t} signals are depicted, superimposed over e_1 and e_2. As Fig. 16 indicates, there is a good fit (however not perfect) between experimental and theoretical EMF signals. There is a *1.5747 rad* phase shift in between, slightly bigger than $\pi/2=1.5707$ rad. This is the explanation for the appearance of the offset component on the NEMF signal.

The using of IAS_{2a} method in NEMF signal processing during the same experiment produces the result from Fig. 17, with a zoom-in detail from area A depicted in Fig. 18 (in the same time interval as Fig. 13).

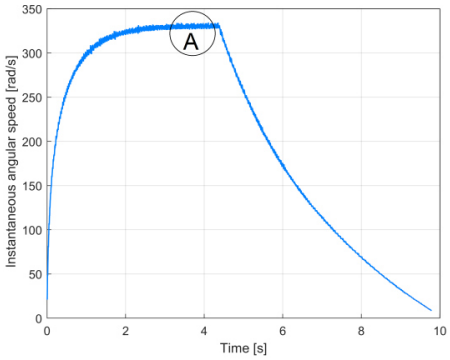


Fig. 17 – The IAS_{2a} evolution deduced from NEMF signal.

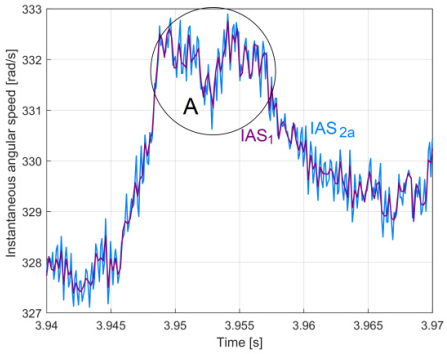


Fig. 18 – A zoom-in detail of 30 ms in area A from Fig. 17.

These last two results prove that the occurrence and the removing method of the DC offset component in NEMF signal (with IAS_{2a} method) are fully confirmed (especially by comparison between Figs. 18 and 13).

A zoom-in detail from area A of Fig. 18 is depicted in Fig. 19.

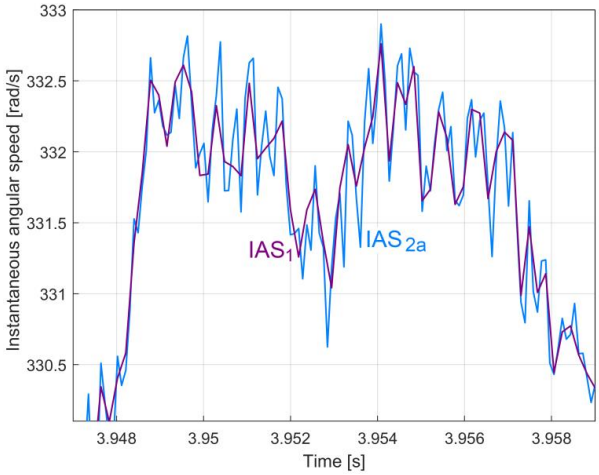


Fig. 19 – A zoom-in detail of 30 ms in area A from Fig. 18.

It is obvious that IAS_{2a} produces two times more samples than IAS_1; the high frequency variable components of IAS are better described, a better approach of condition monitoring of rotary machines is possible using IAS_{2a}. The IAS_1 evolution in Fig. 17 has 32,182 samples while IAS_{2a} has 64,366 samples.

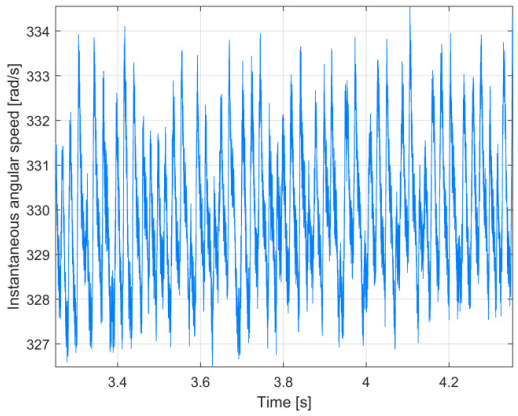


Fig. 20 – A zoom-in detail of the stationary regime area in Fig. 17.

If in condition monitoring of stationary regimes the fast Fourier transform (FFT) is used, then the upper limit of the frequency in FFT spectrum (Nyquist frequency) is two times larger in IAS_{2a} compared to IAS_1.

Suppose we have a short sequence of both IAS evolutions in stationary regime in area A in Fig. 17 (from *t=3.25 s* to *t=4.35 s*), depicted in Fig. 20 (with 5,795 IAS_1 samples and 11,590 IAS_{2a} samples) with an average IAS of 329.9 rad/s (for *f =52.505 Hz* as rotation frequency).

For IAS_1 method, with 100 samples per rotation, there are 5250.5 samples per second in IAS description. Half of this frequency (2625.25 Hz) is the upper limit (Nyquist frequency) for IAS_1 FFT spectrum.

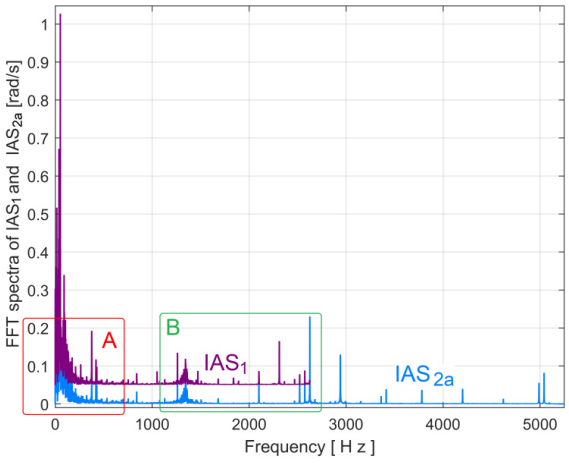


Fig. 21 – The FFT spectra of the IAS_1 and IAS_{2a} evolutions from Figure 20.

For IAS_{2a} method, with 200 samples per rotation, there are 10501 samples per second in IAS description. Half of this frequency (5250.5 Hz) is the upper limit (Nyquist frequency) for IAS_{2a} FFT spectrum.

These considerations are fully confirmed in the description of spectra from Fig. 21 related with the FFT (with real amplitudes) of the evolutions depicted in Fig. 20 (here the IAS_1 spectrum is artificially

shifted up with 0.05 rad/s, to make-it more visible).

Both spectra (having high similarities) prove that IAS signal delivered by this sensor is deterministic (with a very low level of noise). Each peak describes a variable sinusoidal component inside IAS, related with the condition of the parts inside the rotary machine, a future topic in our research.

A zoom-in detail on area A of Fig. 21 (depicted in Fig. 22) reveals that the dominant sinusoidal component in IAS (52.56 Hz frequency) has roughly the same frequency with the average frequency of rotary machine rotation (52.505 Hz, already mentioned in the comments of Fig. 20). The difference in between is generated by a bad resolution in frequency of the spectrum (0.906 Hz, this being the gap frequency between any two successive samples in spectrum), due to a small number of IAS samples from Fig. 20. This dominant component (as highest peak on spectrum) proves mainly that there is a variation of mechanical loading of the electric hand drill chuck on its rotation frequency, running in idle (the increasing of loading produces a decreasing of IAS and the other way around). Certainly this dominant component is also related by the sensor itself, more precisely due to mechanical, electrical or magnetic asymmetries in its construction.

Some other peaks on Fig. 21 describe other relevant sinusoidal components inside the IAS signal. A zoom-in detail in area B of Fig. 21 (depicted in Fig. 23) reveals that at high frequency some peaks on IAS_{2a} are missing. There is no reasonable explanation for this inconvenient. Here it is also available the upper limit of IAS_1 spectrum and a significant peak on 2626 Hz frequency, as the 50^{th} harmonic of the rotation frequency.

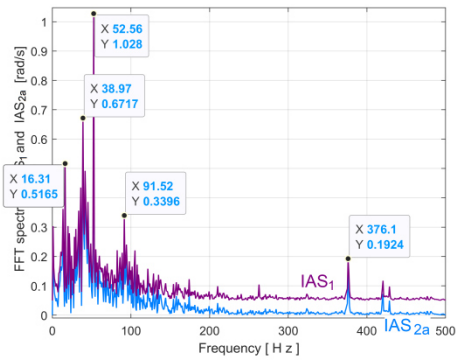


Fig. 22 – A zoom-detail in area A of Fig. 21.

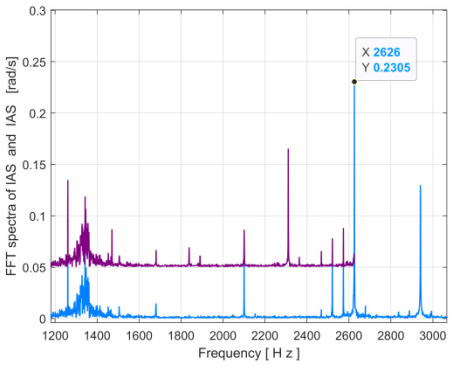


Fig. 23 – A zoom-detail in area B of Fig. 21.

The better explanation regarding the existence of this peak is the fact that the both EMF signals have 50 periods on each rotation of the sensor rotor (or of the electric hand drill chuck as well).

5. Conclusions and future work

A new approach in IAS monitoring using a stepper motor as rotation sensor (acting as a two-phase *n=50* poles AC generator) is proposed. During rotation motion, on each phase a sinusoidal EMF signal is generated (theoretically in phase quadrature each other). The paper proposes a way to increase the sampling rate of IAS numerical description from 100 to 200 samples per sensor rotor rotation (the conversion of the sensor in virtual single-phase *2n=100* poles AC generator). The mathematical product of two EMF signals generated by the real sensor defines a new EMF signal (NEMF). Its overlapped periods are used in this new IAS description method (as IAS_{2a}). This overlapping (equal to a semi-period between two successive periods) is necessary in order to eliminate the negative influence of a DC offset in the NEMF signal on the IAS description.

For a rotation frequency *f*, the IAS_{2a} method has a high sampling rate (*200·f*) so the Nyquist limit is *100·f*, which is a good opportunity for condition monitoring of rotary machines using FFT spectrum evolution.

Some experimental achievements in IAS monitoring were used to validate the theoretical approach.

In the future we will look forward for a method to eliminate the inaccuracy in IAS measurement generated by sensor construction asymmetries.

REFERENCES

Bourdon A., André H., Rémond D., *Introducing angularly periodic disturbances in dynamic models of rotating systems under non-stationary conditions*, Mech. Syst. Signal. Process., **44**, 60-71 (2014).

Bourogaoui M., Sethom H.B.A., Belkhodja I.S., *Speed/position sensor fault tolerant control in adjustable speed drives – A review*, ISA Transactions, **64**, 269-284 (2016).

Bumbu N.E., Horodincă M., *The mirroring of a transient regime of a lathe headstock gearbox in the evolution of supplying voltage of the AC driving motor*, Recent **23**, 1, 21-30 (2022).

Horodincă M., Ciurdea I., Chitariu D.F., Munteanu A., Boca M., *Some approaches on instantaneous angular speed measurement using a two-phase n poles AC generator as sensor*, Measurement **157**, 107636 (2020).

Ciurdea I., Horodincă M., *Instantaneous angular speed measurement and signal processing: a brief review*, Bul. Inst. Polit. Iaşi, s. Machin Manufact., **63** (67), 1, 51-73 (2017).

Ciurdea I., Horodincă M., *Instantaneous angular speed monitoring based on signal amplitude of an AC generator used as sensor*, Bul. Inst. Polit. Iaşi, s. Machin Manufact., **64** (68), 2, 15-26 (2018).

Guo Y., Li W., Yu S., Han X., Yuan Y., Wang Z., Ma X., *Diesel engine torsional vibration control coupling with speed control system*, Mech. Syst. Signal. Process., **94**, 1-13 (2017).

Kim D., Park J., *Application of adaptive control to the fluctuation of engine speed at idle*, Inform. Science, **177**, 3341-3355 (2007).

Li B., Zhang X., Wu J., *New procedure for gear fault detection and diagnosis using instantaneous angular speed*, Mech. Syst. Signal. Process., **85**, 415-428 (2017).

Li Y., Gua F., Harris G., Ball A., Bennett N., Travis K., *The measurement of instantaneous angular speed*, Mech. Syst. Signal. Process., **19** (4), 786-805 (2005).

Lei Y., Lin J., Zuo M., He Z., *Condition monitoring and fault diagnosis of planetary gearboxes: A review*, Measurement, **48**, 292-305 (2014).

Sarma S., Agrawal V.K., Udupa S., Parameswaran K., *Instantaneous angular position and speed measurement using a DSP based resolver-to-digital converter*, Measurement, **41**, 788-796 (2008).

Zhao M., Jia X., Lin J., Lei Y., Lee J., *Instantaneous speed jitter detection via encoder signal and its application for the diagnosis of planetary gearbox*, Mech. Syst. Signal. Process., **98**, 16-31 (2018).

O ÎMBUNĂTĂȚIRE A MONITORIZĂRII VITEZEI UNGHIULARE INSTANTANEE PRIN INTERMEDIUL SEMNALELOR EMF SINUSOIDALE FURNIZATE DE UN GENERATOR DE CURENT ALTERNATIV CU DOUĂ FAZE ȘI *n* POLI, UTILIZAT CA SENZOR

(Rezumat)

În lucrare se prezintă o nouă metodă de constituire a informației de descriere a vitezei unghiulare instantanee pe baza semnalelor EMF (ca tensiuni sinusoidale) generate de un generator cu două faze și *n=50* poli. Drept senzor este utilizat un motor pas cu pas în regim de generator. Semnalele EMF (50 perioade pe rotația rotorului senzorului) generate pe fiecare dintre cele două faze (aflate în quadratură de fază) se înmulțesc matematic, generându-se un semnal sinusoidal (NEMF) cu frecvență dublă (100 de perioade pe rotația rotorului senzorului). Utilizarea perioadelor succesive din semnalul NEMF (cu suprapunere de o semi-perioadă) permite definirea a 200 de eșantioane de viteză unghiulară instantanee pe rotația rotorului. Utilizarea perioadelor din NEMF (și nu a semi-perioadelor) rezolvă o problemă importantă: eliminarea efectelor componentei de ofset din NEMF generată din cauza faptului că semnalele EMF (din care se constituie semnalul NEMF) nu sunt strict în cuadratură de fază.

Noua metodă de constituire a informației de viteză unghiulară instantanee crește rata de descriere a acesteia de la *100·f* la *200·f*, cu *f* frecvența de rotație a rotorului senzorului. Se dublează astfel și frecvența Nyquist care limitează spectrul obținut prin utilizarea transformatei rapide Fourier la conversia din domeniul timp în domeniul frecvență (pentru situațiile de monitorizare și diagnoză a stării sistemelor mecanice rotative).

În lucrare sunt prezentate elemente de suport teoretic și unele ilustrări experimentale de validare a acestora.